Applied Surface Science 301 (2014) 134–141

Contents lists available at ScienceDirect

Applied Surface Science

journal homepage: www.elsevier.com/locate/apsusc

# $Ag_2S$ deposited on oxidized polypropylene as composite material for solar light absorption

Valentina Krylova[a], Alexander Milbrat[b], Anika Embrechts[c], Jonas Baltrusaitis[b,*]

[a] Department of Inorganic Chemistry, Kaunas University of Technology, Radvilenu St. 19, LT-50254 Kaunas, Lithuania
[b] PhotoCatalytic Synthesis Group, MESA+ Institute for Nanotechnology, Faculty of Science and Technology, University of Twente, Meander 229, PO Box 217, 7500 AE Enschede, The Netherlands
[c] Saxion University of Applied Sciences, Research Centre for Design and Technology, Section Nanotechnology, M.H. Tromplaan 28, 7513 AB Enschede, The Netherlands

ARTICLE INFO

*Article history:*
Received 19 August 2013
Received in revised form 3 February 2014
Accepted 3 February 2014
Available online 15 February 2014

*Keywords:*
Silver sulfide
Oxidized polypropylene
Chemical bath deposition
XPS
AFM

ABSTRACT

Thin film metal chalcogenides are superior solar light absorbers and can be combined into a functional material when deposited on polymeric substrates. $Ag_2S$ composite materials were synthesized on oxidized polypropylene using chemical bath deposition method and their properties were explored using XRD, XPS, AFM and UV–Vis. Polypropylene surfaces were modified using solution methods to introduce hydrophilicity via carboxylic group formation which resulted in $Ag_2S$ film deposition and adhesion. These films showed slightly sulfur enriched composition from XPS analysis with the sulfate-like species forming, presumably at the oxidized polymer surface sites. $Ag_2S$ particle growth mechanism included nucleation and rather large (few μm) aggregate formation eventually covering the complete polymer surface, as inferred from AFM analysis. Absorption edge of the composite material shifted toward the higher wavelength in UV–Vis spectrum with the number of $Ag_2S$ exposure times showing a decreasing bandgap and the possibility of obtaining tunable optical property $Ag_2S$–polymer composites using CBD methods.



## Introduction

The rapid growth of the world economy as well as the Earth's population puts a strict requirement toward the new way and methods for inexpensive energy generation. Renewable energy sources, such as solar, wind, hydro and biomass recently have attracted significant amount of attention. Among these alternatives, conversion of solar light into electrical energy has become the most popular due to the large surplus of solar radiation available. Each year, 120.000 TW of solar radiation strikes the Earth's surface. For comparison, the global annual energy consumption is 13.5 TW, and is expected to increase to about 30 TW by the 2050 [1,2], which means that an immense potential lies in harvesting solar energy. However, using our current technologies, providing 30% of global energy needs in 2050 would require to cover an area of 250.000 $km^2$ with semiconductors even assuming an optimistic 10% solar-to-hydrogen conversion efficiency [3]. This surface area implies tremendous amounts of solar absorber material, while also invoking their corresponding efficiency, cost and availability criteria. In the latest considerations, non-metal oxide based materials, such as sulfides are proposed to convey the highest electricity potential vs. materials cost ratio [4,5].

To minimize the amount of the solar absorber material, thin films of high absorptivity need to be considered. Silver sulfide ($Ag_2S$) is an important metal chalcogenide semiconductor compound with the band gap of ~1.5 eV [6] and a high absorption coefficient of approximately $10^4$ $cm^{-1}$ [7], able to ensure most of the solar light absorption in a thin layer. $Ag_2S$ belongs to I–VI compound semiconductor materials with monoclinic crystal structure. It possesses a unique combination of properties, such as high dark ionic or electronic conductivity, photoconductivity, as well as related photovoltaic and photochromic effects [6,8–10]. Silver sulfide thin films have been produced as functional materials with applications in the contemporary advanced technologies ranging from photoconductive and photovoltaic cells, solar selective coatings, ion selective electrodes and membranes to IR detectors and laser recording media [11–18].

Composite materials consisting of polymers covered by thin layers of inorganic compounds possess tunable characteristic optical and semiconducting properties. In the recent years, metal

* Corresponding author. Tel.: +31 53 489 3968.
*E-mail addresses:* valentina.krylova@ktu.lt (V. Krylova), a.milbrat@utwente.nl (A. Milbrat), a.embrechts@saxion.nl (A. Embrechts), j.baltrusaitis@utwente.nl (J. Baltrusaitis).

http://dx.doi.org/10.1016/j.apsusc.2014.02.014
0169-4332/

chalcogenide semiconducting thin films on polymeric surfaces have been extensively studied due to their technological importance. Polypropylene is one of the fastest growing classes of thermoplastics and can serve as a model metal chalcogenide–polymer composite. It is low cost, low density, and has high heat distortion temperature (HDT). However, in its intrinsic state, hydrophobic polypropylene does not possess the surface properties required for preparation of thin solar absorber film composites. Polypropylene is resistant toward many solvents and chemicals. It is known due to its apolar characteristics, which has direct influence on its adhesion properties [19–22]. One of the polypropylene surface modification methods is its oxidation. The oxidation of isotactic polypropylene (iPP) in solid phase has been done via reactions with ozone, γ-initiated corona method and UV ray or with chemical oxidizing mixture [19,23–30]. The oxidation of iPP leads to the formation of oxygen-containing surface functional groups, which greatly affect the surface polarity and the adhesion properties of the polymer toward the metal chalcogenide deposition.

Thin film solar light absorbers are of particular interest for fabrication of large area arrays, solar selective coatings and solar cells. As such, tuneable and controllable thickness thin film deposition is of crucial importance in attaining their desired absorbing. Previously, $Ag_2S$ thin films with different morphologies have been prepared via various methods, such as solid–vapor reactions [31], radio frequency sputtering [32], thermal evaporation [33], electro deposition [34], successive ionic layer absorption and reaction (SILAR) [35] and chemical bath depositions (CBD) [6]. As in most of metal sulfide materials, a crucial property for solar energy harvesting is the resulting conductivity. It has already been shown that elemental stoichiometry affects the conductivity of sulfide thin films. Pyrite, $FeS_2$, for example, has been proposed as the next potentially efficient, abundant and inexpensive solar absorber [5]. However, tiny differences in elemental composition via sulfur defect states have been shown to affect the semiconducting properties of pyrite tremendously [36]. Consequentially, methods of solar absorber $Ag_2S$ thin films need to be obtained for a reproducible thin films with the desired stoichiometry. Compared with other deposition methods, previously proposed modification of the chemical bath deposition technique is very convenient, facile, low cost and environmentally friendly [30,37]. This is due to the fact that $Ag_2S$ sediments can be re-used after the reaction since they redissolve in nitric acid [37].

In this study, $Ag_2S$ thin films were synthesized on the partially oxidized hydrophilic polymeric material – isotactic polypropylene (iPP) – using chemical bath deposition. This method is based on a controlled precipitation of the desired compound from its corresponding ions in the reaction bath solution. While $Ag_2S$ has previously been deposited on hydrophilic or partially hydrophilic polymers, such as polyamide [37], here we employ hydrophobic polymer – polypropylene – as a substrate. Oxidized polypropylene – which possesses a hydrophilic character – was also prepared and structurally characterized to provide maximum adhesion for the $Ag_2S$ material. Structural, chemical and optical properties of the resulting composite materials were determined using XRD, XPS, UV–Vis and AFM.

## Experimental methods

### *Materials*

All solutions were prepared using distilled water and analytical grade reagents. Only freshly prepared solutions were used for measurements and were not de-aerated during the experiments. $H_2SO_4$ (96%, Barta a Cihlar, Czech Republic), $H_3PO_4$, (60%, Lach-Ner, Czech Republic), $CrO_3$ (>99%, Reachim, Russia), sodium thiosulfate ($Na_2S_2O_3{\cdot}5H_2O$) (>99%, Sigma-Aldrich, Germany), and $HNO_3$ (65%, Penta, Czech Republic) were used as received.

### *Polypropylene oxidation*

Isotactic polypropylene (iPP) used in this study was supplied by KWH Plast (Finland). 15 × 70 mm samples of non-oriented isotactic polypropylene film of 150 μm thickness were used for these experiments. First, polypropylene surface was oxidized to obtain hydrophilic properties for silver sulfide adhesion to proceed. Surface of the commercial iPP samples was treated for 25 min at 90 °C with oxidizing solution consisting of $H_2SO_4/H_3PO_4$ (1:1, saturated with $CrO_3$) and finally rinsed with distilled water.

### *$Ag_2S$ deposition on oxidized polypropylene*

$Ag_2S$ deposition on oxidized polypropylene was performed using procedures described previously for polyamide substrate [37]. Briefly, samples of the oxidized iPP were treated with aqueous $Na_2S_2O_3$ (0.2 mol/dm$^3$) and $AgNO_3$ (0.06 mol/dm$^3$) solution at 20 °C with pH 2.3 (by adding nitric acid). All reactions of iPP treatment were carried out in the glass reactor. iPP films were immersed for 40 min up to six times in the precursor solution. Samples were withdrawn at certain time intervals, rinsed with the distilled water, dried with filter paper, left over anhydrous $CaCl_2$ for 24 h and then used in analysis. Throughout the text, index added to the iPP-$Ag_2S$ represent the number of immersions with iPP-$Ag_2S$-1, iPP-$Ag_2S$-2, iPP-$Ag_2S$-3, iPP-$Ag_2S$-4, iPP-$Ag_2S$-5 and iPP-$Ag_2S$-6 corresponding to 1, 2, 3, 4, 5 and 6 immersions, respectively.

### *XPS and AFM analysis*

XPS surface elemental analysis of the iPP-$Ag_2S$ composites was performed using a custom-designed Kratos Axis Ultra X-ray photoelectron spectroscopy system [38]. The surface analysis chamber is equipped with aluminum $K_\alpha$ X-ray gun and 500 mm Rowland circle silicon single crystal monochromator. The X-ray gun was operated using a 15 mA emission current at an accelerating voltage of 15 kV. Low-energy electrons were used for charge compensation to neutralize the sample. High-resolution spectra were acquired in the region of interest using the following experimental parameters: 20–40 eV energy window; pass energy of 20 eV; step size of 0.1 eV, and dwell time of 1000 ms. One sweep was used to acquire a survey spectrum of all binding regions. The absolute energy scale was calibrated to the Cu $2p_{2/3}$ peak binding energy of 932.6 eV using an etched copper plate. All spectra were calibrated using the adventitious C 1s peak at 285.0 eV. A Shirley-type background was subtracted from each spectrum to account for inelastically scattered electrons that contribute to the broad background. CasaXPS software was used to process the XPS data [39]. Transmission corrected relative sensitivity factor (RSF) values from the Kratos library were used for elemental quantification. An error of ±0.2 eV is reported for all peak binding energies.

Atomic force microscopy height images were obtained using a Bruker Multimode 8 (NanoScope V controller) in tapping mode and Peakforce QNM mode. A Bruker TAP150 (MPP-12100) rectangular beam cantilever was used with a nominal spring constant of 5 N/m for the iPP-$Ag_2S$-1 and iPP-$Ag_2S$-3 samples (Peakforce QNM mode). A Bruker TAP525 (MPP-13100) rectangular beam cantilever was used with a nominal spring constant of 200 N/m for the iPP-$Ag_2S$-6 samples (tapping mode). Image analysis was performed using Bruker Nanoscope Analysis 1.40. For the particle analysis a threshold was used which allowed for particle recognition on the image. A bin size of 50 bins was chosen in each case.

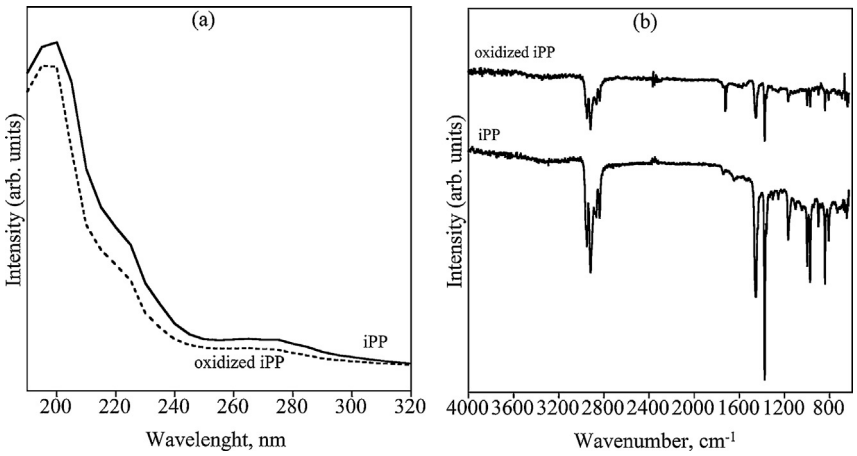


**Fig. 1.** (a) UV–Vis and (b) transmission ATR–FTIR spectra of commercial and oxidized iPP samples.

*Other instruments and methods*

*Solution pH*

Solution pH was measured by using pH-meter *WTW330* with combinative glass and Ag/AgCl electrode and temperature meter WTW SenTix 41 (Germany).

*XRD analysis*

X-ray diffractometry was carried out using a Brag Brendan circuit on a Dron-6 diffractometer (Russia) utilizing Cu $K_\alpha$ radiation ($\lambda$ = 0.154178 nm), 30 kV voltage and 30 μA current. The scanning range was $2\theta$ = 25–60° and the scanning speed was 1° $min^{-1}$.

*UV–Vis measurements*

The UV–Vis spectra (200 to 1100 nm) of the iPP-$Ag_2S$ composites were recorded using a Spectronic Genesys 8 UV/Visible spectrophotometer with compensation for iPP absorption while iPP (190–320 nm)—without compensation.

*ATR–FTIR measurements*

ATR–FTIR measurements were performed using Perkin Elmer FT-IR Spectrum GX spectrophotometer by averaging 64 scans with a wavenumber resolution of 0.3 $cm^{-1}$ at room temperature. Spectra were recorded in the wavenumber range 4000–600 $cm^{-1}$.

## Results and discussion

*Surface properties of the oxidized iPP films*

A critical part of iPP modification is its surface preparation via partial oxidation to ensure adhesion with the $Ag_2S$. When iPP was treated with oxidizing solution consisting of $H_2SO_4/H_3PO_4$ (1:1) saturated with $CrO_3$, a chemical reaction took place on the surface of the sample, as signified by the changes in UV–Vis and ATR–FTIR spectra shown in Fig. 1a and b, respectively. UV–Vis absorption spectrum of iPP shown in Fig. 1a contains three absorption peaks at 200 nm and less intense and shallower bands at 225 and 265 nm. Since iPP ideally contains only C–H and C–C bonds, no features in UV–Vis spectra should be observed. However, residual impurities and surface carbonyl groups can be present which might yield peaks observed. These carbonyl groups are responsible for 265 nm peak [40] and slightly decreased in intensity with oxidative treatment via carbonyl conversion to OH bond containing species. It can also be seen that the intensity of the absorption peak at ~195 nm, which indicates the existence of polar group in the polymer matrix [41]. Thus it can be inferred, that oxidizing type of treatment causes subtle change in the chemical structure of the polymer without resulting in its altered major physical and structural properties.

Introduction of additional polar groups on the iPP sample surface was probed via ATR–FTIR which due to the evanescent wave penetration depth has a probing depth of ~5 μm. ATR–FTIR spectra of as received iPP and oxidized iPP samples in the range of 4000 to 600 $cm^{-1}$ can be seen in Fig. 1b. ATR–FTIR spectrum of as received iPP sample reveals strong absorption in the range 2840–3000 $cm^{-1}$ due to $sp^3$ C–H stretch, along with the strong bands near 1458 and 1376 $cm^{-1}$ due to absorptions of $CH_2$ and $CH_3$ groups, respectively, which are characteristics of polypropylene. The absorption features at 840, 1000 and 1170 $cm^{-1}$ are characteristic vibrations of terminal unsaturated $CH_2$ groups present in isotactic iPP which agree well with the reported literature data [42]. Most importantly, ATR–FTIR spectrum of oxidized iPP sample exhibits a noticeable change. The characteristic peaks of iPP sharply decrease in intensity. Also, a band starts growing near 1715 $cm^{-1}$ that indicates the presence of C=O bonds [41]. The spectrum of oxidized iPP confirms that the oxidizing treatment of polypropylene increases surface hydrophilicity by introducing oxygen containing polar groups. Higher hydrophilicity of iPP surface causes electrostatic interactions between the charged surface of the polymer and the silver sulfide particles, providing better adhesion, a critical parameter in such composite preparation.

*XRD analysis of iPP-$Ag_2S$ composite materials*

The deposited $Ag_2S$ layers were subjected to XRD analysis to investigate their crystallographic structure. XRD difractograms of samples were recorded in the $2\theta$ range between 25° and 60°. Fig. 2 shows the X-ray diffraction pattern of the iPP-$Ag_2S$ composites. After the first exposure in the precursor solution, the diffraction pattern of deposits on the polypropylene sample gave dominant peaks $2\theta$ at 26.2°, 29.1°, and 43.5°. After more exposures and when analysis of the scrapings of the iPP-$Ag_2S$-6 sample was performed, diffraction pattern gave dominant peaks $2\theta$ at 26.2° (the crystallographic plane (1 1 1)), 29.1° (0 1 2), 31.8° (1 2 0), 33.7° (1 2 1), 34.7° (1 1 2), 36.8° (0 2 2), 37.7° (2 0 0), 40.8° (0 3 1), 43.5° (1 3 0), 45.5° (−1 3 1), 48.8° (0 1 4), 46.3° (2 0 2), 47.8° (−2 1 2), and 53.2° (0 0 4). The diffraction patterns were indexed to the monoclinic $Ag_2S$ phase and are in good agreement with the reported data for α-$Ag_2S$ (acanthite) (JCPDS Card File: 00-014-0072). Crystallite size of the $Ag_2S$ in iPP-$Ag_2S$ composite materials was calculated using Sherer's formula [43]

$$D_{hkl} = \frac{0.89\lambda}{\beta \cos\theta}$$

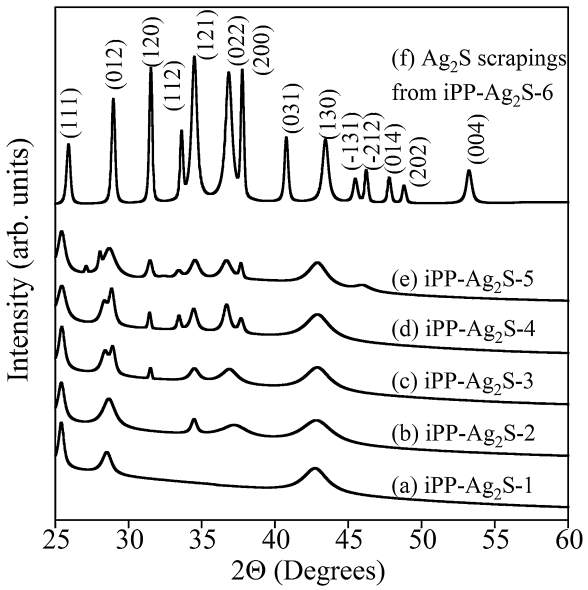


**Fig. 2.** Representative XRD patterns of iPP-$Ag_2S$-1, iPP-$Ag_2S$-2, iPP-$Ag_2S$-3, iPP-$Ag_2S$-4, iPP-$Ag_2S$-5 composites. The number on the pattern represents number of exposures. In addition, XRD pattern of surface deposits from the iPP-$Ag_2S$-6 composite is shown. Peaks observed are those of acanthite, $Ag_2S$ (JCPDS Card File: 00-014-0072).

where $D$ is the average crystallite size, nm, $\lambda$ is the X-ray wavelength, ($\lambda$ = 1.54178 Å), $\beta$ is the FWHM of the diffraction peak, $2\theta$ is the diffraction angle. Typical crystallite size calculated ranged from 50 to ~300 nm, depending on a peak. While it is difficult to accurately calculate the crystallite size due to the low intensity of the peaks on an intense iPP background, size range obtained is within the few hundred nanometers.

**Table 1**
Atomic concentration calculations for iPP-$Ag_2S$ samples obtained from XPS analysis.

| Sample | Ag 3d (%) | S 2p (%) | S (%) | $S^{2-}$ (%) | $SO_4^{2-}$ (%) |
|---|---|---|---|---|---|
| iPP-$Ag_2S$-1 | 63 | 37 | 9 | 70 | 21 |
| iPP-$Ag_2S$-2 | 66 | 34 | 18 | 75 | 7 |
| iPP-$Ag_2S$-3 | 65 | 35 | 20 | 73 | 8 |
| iPP-$Ag_2S$-4 | 63 | 37 | 15 | 71 | 14 |
| iPP-$Ag_2S$-5 | 58 | 42 | 21 | 58 | 21 |
| iPP-$Ag_2S$-6 | 61 | 39 | 18 | 63 | 19 |

*Chemical surface composition of iPP-$Ag_2S$ composite materials*

XPS spectra of iPP-$Ag_2S$ films showed information, typical to that of PA-$Ag_2S$ composite materials recently reported [37]. Representative XPS spectra of iPP-$Ag_2S$ composite material after six exposures (iPP-$Ag_2S$-6) are shown in Fig. 3. Ag $3d_{5/2}$ peak for all the samples analyzed was located at 368.2 eV, close to the 368.0 eV value reported for bulk $Ag_2S$ powder [44,45]. Corresponding S 2p doublet with S $2p_{3/2}$ peak at 161.4 eV confirms $Ag_2S$ formation [44,45]. Similar to the previous work, two additional sulfur species were found on all sample surfaces with S $2p_{3/2}$ peaks located at 163.5 and 168.0 eV. The origin of the former peak was discussed previously [37] and several assignments have been proposed, including $S_2O_3^{2-}$ or $S_4O_6^{2-}$ species [46,47], or oxygen–sulfur on substoichiometric metal sulfides [48]. Differently from the previous work, another species formed on PA-$Ag_2S$ surface with S $2p_{3/2}$ peak at 168.0 eV cannot be unambiguously due to $S^{+6}$ in $SO_4^{2-}$ [38,49]. While it is certainly a very oxidized type of sulfur species, all of the sulfate species reported in the literature are typically observed at 168.8 eV and higher. We attribute this peak due to the sulfate bonded to the oxidized iPP sites. Table 1 shows the quantification of Ag:S, as well as a distribution of sulfur species. Initial few stages of deposition resulted in almost stoichiometric $Ag_2S$ whereas at the latter stages surplus of sulfur can be observed, differently from the stoichiometric value of 2:1. It is possible that additional

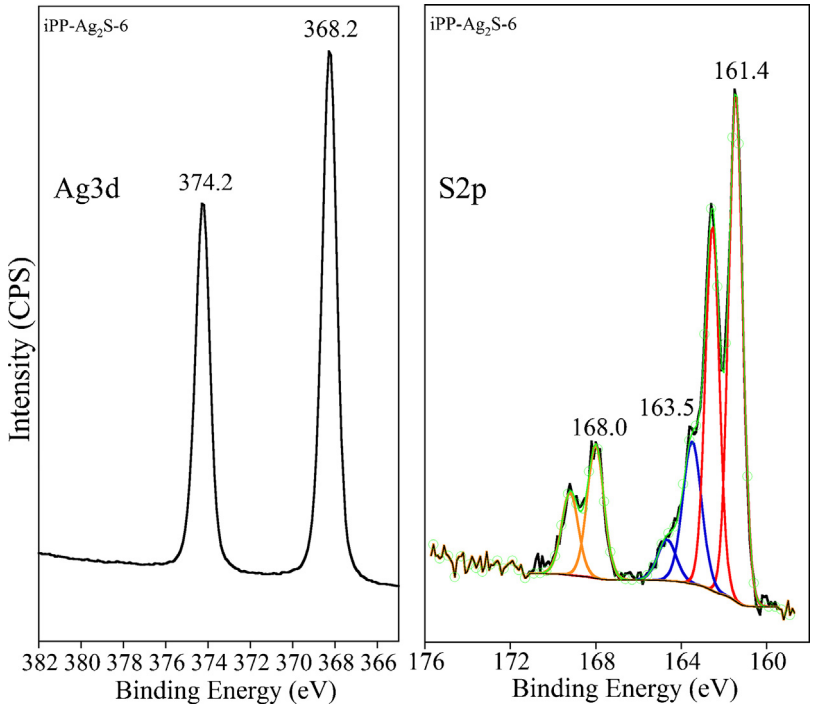


**Fig. 3.** A representative XPS spectra of iPP-$Ag_2S$ composite materials. That for iPP-$Ag_2S$-6 is shown. Different colors show doublets due to the different chemical species present.

**Table 2**
Measured mass increase for the complete deposition series for a typical iPP sample of 1.5 × 4 cm (6 $cm^2$ area).

| Sample | Sample mass (g) | Mass increase (g) | Mass increase (%)[a] |
|---|---|---|---|
| iPP | 0.082 | – | – |
| iPP-$Ag_2S$-1 | 0.0915 | 0.0095 | 11.6 |
| iPP-$Ag_2S$-2 | 0.0934 | 0.0019 | 2.1 |
| iPP-$Ag_2S$-3 | 0.0955 | 0.00206 | 2.2 |
| iPP-$Ag_2S$-4 | 0.0976 | 0.0021 | 2.2 |
| iPP-$Ag_2S$-5 | 0.0999 | 0.0023 | 2.3 |
| iPP-$Ag_2S$-6 | 0.1017 | 0.0018 | 1.8 |

[a] Calculated as $(mass_{n+1} - mass_n/mass_n) \times 100$.

chemistry proceeds at the oxidized iPP surface sites yielding species with S $2p_{3/2}$ peaks located at 163.5 and 168.0 eV slightly increasing sulfur amount observed. Furthermore, presence of oxidized sulfate species seems to be significant in the first sample, as well as the higher exposure ones. According to the AFM studies reported here (*vide infra*), very thin layers are initially formed on top of iPP (spherulites of iPP can clearly be discerned). Additional exposures lead to more homogeneous layers where iPP seems to be fully covered by a thin layer of $Ag_2S$, since the spherulitic structure of iPP is barely visible. XPS data for iPP-$Ag_2S$-4 through iPP-$Ag_2S$-6 shows very similar surface speciation, albeit at somewhat large distribution. It can be due to the samples forming surface in macroscopically inhomogeneous fashion during the drying stage, as shown in previous SEM studies of copper selenide deposition on polyamide [50].

Typically, when polymer surfaces are treated using the method described here to deposit metal sulfide or selenide films, thin self-limiting films of ~5 μm result [37,50]. In the present experiments, we measured a mass increase of the samples after every exposure with the data tabulated in Table 2. Largest mass increase resulted after the unreacted oxidized iPP was exposed to the precursor solution the first time with about 11.6% increase. Every exposure that followed further contributed about ~2% of the mass increase. Using these numbers and $Ag_2S$ density of 7.22 g/$cm^3$ [51], we calculate ~0.46 μm thickness layer grown during the first exposure and ~0.23 μm thickness layer grown during each consecutive cycle. Actual film thickness of pure $Ag_2S$ phase can be less since some of the material will initially diffuse into the iPP before forming surface films [37,50] but the bulk density value used in calculations may not accurately describe that of the iPP-$Ag_2S$ composite. This thickness agrees well with that needed for novel thin film solar cell materials as metal sulfides in general have high absorption coefficient ($10^4$ $cm^{-1}$) [52]. These diffused films are at the core of the hybrid thin film solar cell concept [53] and can be prepared using the method described here using virtually any hydrophilic polymer substrate or, as in the case described in this work, even hydrophobic polymer after its surface has been treated to induce hydrophilicity.

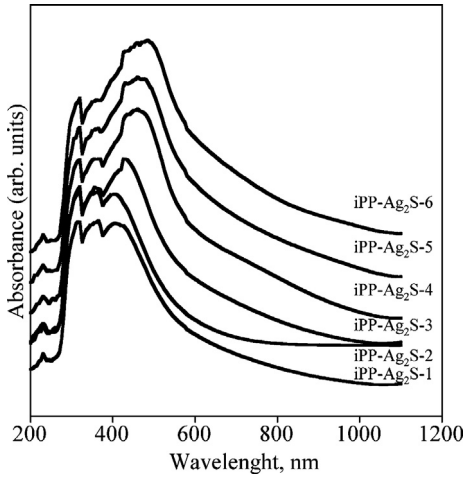


**Fig. 4.** UV–Vis spectra of iPP-$Ag_2S$ composites as a function of the exposure number.

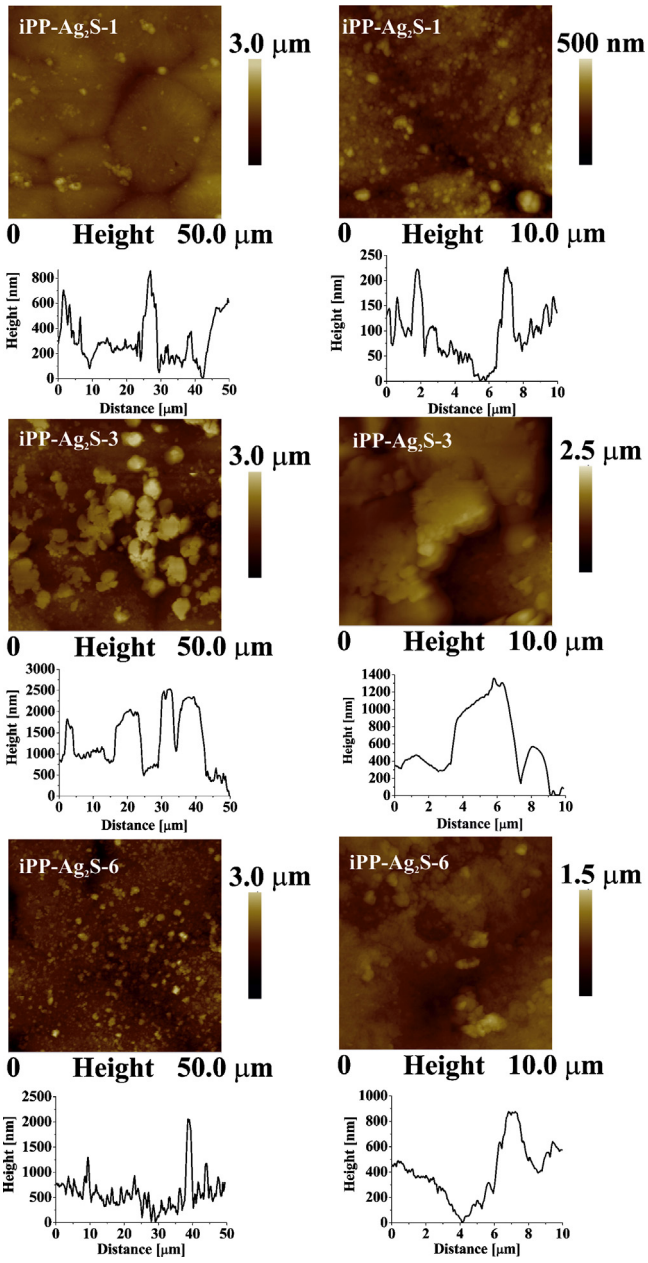


**Fig. 5.** AFM topography images of iPP-$Ag_2S$-1, iPP-$Ag_2S$-3 and iPP-$Ag_2S$-6 samples.

### *Optical and morphological analysis of iPP-$Ag_2S$ composite materials*

UV–Vis spectra of iPP-$Ag_2S$ composite materials were obtained and are shown in Fig. 4. After interaction of silver ions with polypropylene in the presence of sulfur, a number of new peaks appear in the interval of 320 to 410 nm. Three obvious absorption peaks at 320, 355, and 410 nm appeared on the surface of iPP (Fig. 4, iPP-$Ag_2S$-1). All these peaks systematically characterize the very basic process of the band structure formation of $Ag_2S$ starting from the nanocluster level. Small silver sulfide particles are first incorporated into the pore systems of the iPP during the crystallization process. With increasing immersions time these particles join

into agglomerates and after six immersions formed entire layer. Therefore after six immersions, in a UV–Vis spectrum is peak at around 500 nm, characteristic $Ag_2S$ (Fig. 4, curve iPP-$Ag_2S$-6). It can also be seen that with the increasing number of deposition steps, absorption maximum shifts from 410 to 500 nm. This transition represents a shift from the iPP peak to the sizeable contribution of $Ag_2S$ in the spectrum itself, as $Ag_2S$ has typical absorbance at around 500 nm [54]. The apparent shift of the 410 nm peak toward higher wavelengths in Fig. 4 also signifies gradual increase in $Ag_2S$ layer thickness and, possibly, an absorption edge change due to the changes in particle size [55]. This opens up a possibility of constructing $Ag_2S$-polymer composite devices with tunable optical properties, using synthesis method described here.

AFM topography analysis was performed on iPP-$Ag_2S$ composite surface and representative scans are shown in Fig. 5 for iPP-$Ag_2S$-1, iPP-$Ag_2S$-3 and iPP-$Ag_2S$-6 samples. It can be seen that iPP-$Ag_2S$-1 exhibits morphological structure typical of polypropylene [56] thus implying that $Ag_2S$ deposition proceeds mostly via diffusion into iPP surface or the surface layer is very thin. Isolated particulate matter of submicron dimensions can be observed as onset of $Ag_2S$ crystal formation. iPP-$Ag_2S$-3, however, possesses aggregates on the surface consisting of micron sized particles which are proposed to be due to the $Ag_2S$. These particles in turn are comprised of submicron size particles. iPP-$Ag_2S$-6 shows similar crystallites, however these crystallites are clearly smaller and more abundant. The different distributions also becomes apparent from the roughness analysis presented below in Table 3 and the particle diameter distribution of the $50 \times 50\,\mu m^2$ scans in Fig. 6. From the roughness values presented in Table 3 it can be seen that the measured roughness increases initially from 66 to 443 nm in $10 \times 10\,\mu m$ scan for iPP-$Ag_2S$-1 and iPP-$Ag_2S$-3, respectively, as a function of exposures, while distinct isolated $Ag_2S$ particles are being formed. Roughness, however, decreases for the later stages

**Table 3**
AFM analysis of iPP-$Ag_2S$-1, iPP-$Ag_2S$-3 and iPP-$Ag_2S$-6 samples.

| Sample | $R_q$ (nm) ($10 \times 10\,\mu m^2$) | $R_q$ (nm) ($50 \times 50\,\mu m^2$) |
|---|---|---|
| iPP-$Ag_2S$-1 | 66 | 221 |
| iPP-$Ag_2S$-3 | 443 | 486 |
| iPP-$Ag_2S$-6 | 148 | 278 |

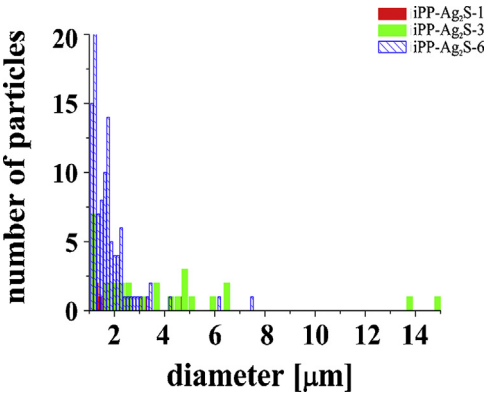


**Fig. 6.** Distribution of the particle sizes of the iPP-$Ag_2S$-1, iPP-$Ag_2S$-3 and iPP-$Ag_2S$-6 samples as obtained from the AFM image analysis.

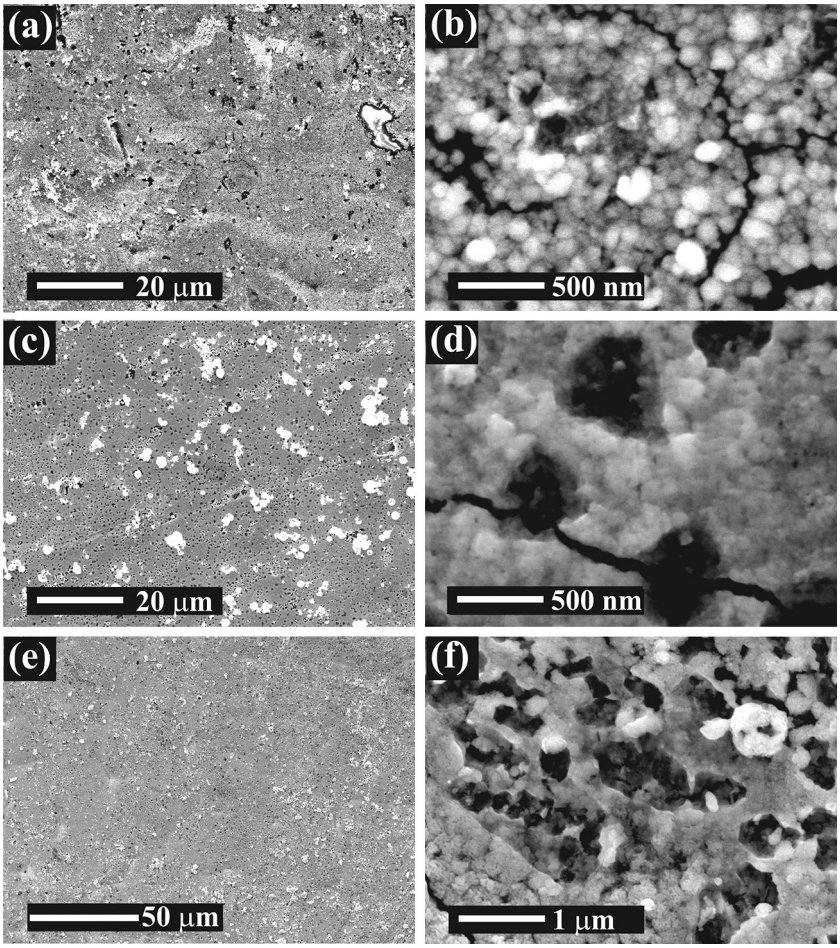


**Fig. 7.** High resolution SEM images of iPP-$Ag_2S$-1 (a and b), iPP-$Ag_2S$-3 (c and d) and iPP-$Ag_2S$-6 (e and f) composite surfaces.

since a more uniform film is being formed. These data suggest that more immersions seem to provide a smoother and more homogenously distributed $Ag_2S$ film on iPP surface. These data are also substantiated by the particle diameter measurements obtained from the AFM images and shown in Fig. 6. It can be seen that mid stages of the depositions, e.g. three exposure sample iPP-$Ag_2S$-3, possesses particles ranging up to 15 μm, while iPP-$Ag_2S$-6 particle diameters are less than 8 μm and a majority below 2 μm. From these data it becomes apparent that $Ag_2S$ does not grow as a uniform film on iPP surface, but rather via nucleation mechanism followed by the particle growth to fill out the complete surface.

High resolution SEM images of iPP-$Ag_2S$-1 (a and b), iPP-$Ag_2S$-3 (c and d) and iPP-$Ag_2S$-6 (e and f) composite surfaces are shown in Fig. 7. It can be seen, that uniform, tight packed films are formed, comprising from ~100 nm $Ag_2S$ nanoparticles. Larger openings are seen within the films of ~0.5 μm in diameter, possibly originating due to the gas bubble emission during the film formation. Small high electron density aggregates can also be discerned on sample surface and result from concentrated $Ag_2S$ material (Fig. 7c), as confirmed by EDS analysis (not shown). These free standing $Ag_2S$ particles most likely result during the drying of the prepared films and are not uniformly present on top of most of the samples.

## Conclusions

$Ag_2S$ on oxidized polypropylene surface was synthesized using chemical bath deposition and the corresponding properties were explored using XRD, XPS, AFM and UV–Vis. We were able to successfully modify iPP surface structure by inducing hydrophilic character via carboxylic group formation which resulted in $Ag_2S$ film deposition and adhesion. $Ag_2S$ films were slightly sulfur rich with a specific sulfate-like species forming on the oxidized polypropylene sites. Absorption peak in UV–Vis shifted with the increasing exposures implying systematically decreasing absorption edge and possibility for a tunable optical property iPP-$Ag_2S$ composites. Atomic force microscopy revealed that increasing number of exposures to precursor solution provided a smoother and more homogenously distributed $Ag_2S$ film on iPP surface. Metal sulfide materials, including acanthite, possess high adsorption coefficients ($10^4\ cm^{-1}$) and will require small film thickness to absorb solar light. When incorporated into polymers using solution methods described here, tunable optical and structural property composites can be obtained.

## Acknowledgments

Authors acknowledge Central Microscopy Research facility at the University of Iowa for XPS time. Lina Samuolaitiene is also acknowledged for the help with the experiments.

## References

[1] Z. Chen, T.F. Jaramillo, T.G. Deutsch, A. Kleiman-Shwarsctein, A.J. Forman, N. Gaillard, R. Garland, K. Takanabe, C. Heske, M. Sunkara, E.W. McFarland, K. Domen, E.L. Miller, J.A. Turner, H.N. Dinh, Accelerating materials development for photoelectrochemical hydrogen production: standards for methods, definitions, and reporting protocols, Journal of Materials Research 25 (2010) 3–16.
[2] N.S. Lewis, D.G. Nocera, Powering the planet: chemical challenges in solar energy utilization, Proceedings of the National academy of Sciences of the United States of America 103 (2006) 15729–15735.
[3] K. Maeda, K. Domen, Photocatalytic water splitting: recent progress and future challenges, Journal of Physical Chemistry Letters 1 (2010) 2655–2661.
[4] F. Alharbi, J.D. Bass, A. Salhi, A. Alyamani, H.-C. Kim, R.D. Miller, Abundant non-toxic materials for thin film solar cells: alternative to conventional materials, Renewable Energy 36 (2011) 2753–2758.
[5] C. Wadia, A.P. Alivisatos, D.M. Kammen, Materials availability expands the opportunity for large-scale photovoltaics deployment, Environmental Science and Technology 43 (2009) 2072–2077.
[6] I.A. Ezenwa, N.A. Okereke, N.J. Egwunyenga, Optical properties of chemical bath deposited $Ag_2S$ thin films, International Journal of Science and Technology 2 (2012) 101–106.
[7] H. Dlala, M. Amlouk, S. Belgacem, P. Girard, D. Barjon, Structural and optical properties of $Ag_2S$ thin films prepared by spray pyrolysis, European Physical Journal—Applied Physics 2 (1998) 13–16.
[8] B.R. Sankapal, R.S. Mane, C.D. Lokhande, A new chemical method for the preparation of $Ag_2S$ thin films, Materials Chemistry and Physics 63 (2000) 226–229.
[9] S.S. Dhumure, C.D. Lokhande, Studies on the preparation and characterization of chemically deposited $Ag_2S$ films from an acidic bath, Thin Solid Films 240 (1994) 1–6.
[10] T.B. Nasrallah, H. Dlala, M. Amlouk, S. Belgacem, J.C. Bernède, Some physical investigations on $Ag_2S$ thin films prepared by sequential thermal evaporation, Synthetic Metals 151 (2005) 225–230.
[11] A.N. Rodríguez, M.T.S. Nair, P.K. Nair, Structural, optical and electrical properties of chemically deposited silver sulfide thin films, Semiconductor Science and Technology 20 (2005) 576–585.
[12] H.-J. Zhai, H.-S. Wang, $Ag_2S$ morphology controllable via simple template-free solution route, Materials Research Bulletin 43 (2008) 2354–2360.
[13] D. Karashanova, K. Starbova, N. Starbov, Microstructure correlated properties of obliquely vacuum deposited $Ag_2S$ thin films, Journal of Optoelectronics and Advanced Materials 5 (2003) 903–906.
[14] Z. Xiaodong, S. Huaqiang, H. Daming, J. Shumin, F. Xun, J. Kui, Room temperature synthesis and electrochemical application of imidazoline surfactant-modified $Ag_2S$ nanocrystals, Materials Letters 62 (2008) 2407–2410.
[15] Y. Umezawa, P. Buhlmann, K. Umezawa, K. Tohda, S. Amemiya, Potentiometric selectivity coefficients of ion-selective electrodes: Part I. Inorganic cations, Pure and Applied Chemistry 72 (2000) 1851–2082.
[16] R.R. Pradhananga, A. Rajbhandari Nyachhyon, Low cost electrochemical sensors for silver, chloride, bromide and iodide ions, Scientific World 6 (2008) 33–36.
[17] P.K. Khanna, Reduction of transition metal salts by SFS: synthesis of copper and silver sulphides, Synthesis and Reactivity in Inorganic, Metal-Organic, and Nano-Metal Chemistry 37 (2007) 805–808.
[18] E.I. Ezema, P.U. Asogwa, A.B.C. Ekwealor, P.E. Ugwuoke, R.U. Osuji, Growth and optical properties of $Ag_2S$ thin films deposited by chemical bath deposition technique, Journal of the University of Chemical Technology and Metallurgy 42 (2007) 217–222.
[19] B.A.R. Tehrani, A.M. Shoushtari, R.M.A. Malek, M. Abdous, Effect of chemical oxidation treatment on dyeability of polypropylene, Dyes and Pigments 63 (2004) 95–100.
[20] M.H. Kunita, E.M. Girotto, E. Radovanovic, M.C. Goncalves, O.P. Ferreira, E.C. Muniz, A.F. Rubira, Deposition of copper sulfide on modified low-density polyethylene surface: morphology and electrical characterization, Applied Surface Science 202 (2002) 223–231.
[21] F. Leroux, C. Campagne, A. Perwuelz, L. Gengembre, Polypropylene film chemical and physical modifications by dielectric barrier discharge plasma treatment at atmospheric pressure, Journal of Colloid and Interface Science 328 (2008) 412–420.
[22] K. Wang, W. Wang, D. Yang, Y. Huo, D. Wang, Surface modification of polypropylene non-woven fabric using atmospheric nitrogen dielectric barrier discharge plasma, Applied Surface Science 256 (2010) 6859–6864.
[23] F.J. du Toit, R.D. Sanderson, Surface fluorination of polypropylene: 2. Adhesion properties, Journal of Fluorine Chemistry 98 (1999) 115–119.
[24] M.L. Steen, A.C. Jordan, E.R. Fisher, Hydrophilic modification of polymeric membranes by low temperature $H_2O$ plasma treatment, Journal of Membrane Science 204 (2002) 341–357.
[25] A.P. Korikov, P.B. Kosaraju, K.K. Sirkar, Interfacially polymerized hydrophilic microporous thin film composite membranes on porous polypropylene hollow fibers and flat films, Journal of Membrane Science 279 (2006) 588–600.
[26] T. Zeiler, S. Kellermann, H. Munstedt, Different surface treatments to improve the adhesion of polypropylene, Journal of Adhesion Science and Technology 14 (2000) 619–634.
[27] K.N. Pandiyaraj, V. Selvarajan, R.R. Deshmukh, C. Gao, Modification of surface properties of polypropylene (PP) film using DC glow discharge air plasma, Applied Surface Science 255 (2009) 3965–3971.
[28] R.V.A. Rowe, M.H. Kunita, M.F. Porto, E.C. Muniz, A.F. Rubira, R.C. Nery, E. Radovanovic, L.T. Taylor, N. Nazem, Low-resistance films of polyimides with impregnated copper sulfide, Journal of Materials Research 16 (2001) 3097–3106.
[29] F. Milde, K. Goedicke, M. Fahland, Adhesion behavior of PVD coatings on ECR plasma and ion beam treated polymer films, Thin Solid Films 279 (1996) 169–173.
[30] V. Krylova, N. Dukstiene, Synthesis and characterization of $Ag_2S$ layers formed on polypropylene, Journal of Chemistry (2013), http://dx.doi.org/10.1155/2013/987879.
[31] J.A. Muñiz-Lerma, J.F. Hernández-Paz, J.R. Farias-Mancilla, P.E. García-Casillas, C.A. Rodriguez-González, Synthesis of hierarchical dorsal spine $Ag_2S$ structures by a solid–vapor reaction: the effect of reagent gas composition, Journal of Nanomaterials (2012), http://dx.doi.org/10.1155/2012/749481.
[32] T.-Y. Hsu, H. Buhay, N.P. Murarka, Characteristics and applications of silver sulfide ($Ag_2S$) films in the millimeter wavelength region, Proceedings of the Society of Photo-Optical Instrumentation Engineers 259 (1980) 38–45.
[33] M.M. El-Nahass, A.A.M. Farag, E.M. Ibrahim, S. Abd-El-Rahman, Structural, optical and electrical properties of thermally evaporated $Ag_2S$ thin films, Vacuum 72 (2004) 453–460.

[34] X.-Y. Guo, S.-Y. Cheng, P.-M. Lu, H.-F. Zhou, Preparation of $Ag_2S$ thin films by electro-deposition, Materials Science Forum 663-665 (2010) 910–913.
[35] U.M. Jadhav, S.R. Gosavi, S.N. Patel, R.S. Patil, Studies on characterization of nanocrystalline silver sulphide thin films deposited by chemical bath deposition (CBD) and successive ionic layer adsorption and reaction (SILAR) method, Archives of Physics Research 2 (2011) 27–35.
[36] H. Tributsch, S. Fiechter, D. Jokisch, J. Rojas-Chapana, K. Ellmer, Photoelectrochemical power, chemical energy and catalytic activity for organic evolution on natural pyrite interfaces, Origins of Life and Evolution of Biospheres 33 (2003) 129–162.
[37] V. Krylova, J. Baltrusaitis, Synthesis and properties of polyamide–$Ag_2S$ composite based solar energy absorber surfaces, Applied Surface Science 282 (2013) 552–560.
[38] J. Baltrusaitis, C.R. Usher, V.H. Grassian, Reactions of sulfur dioxide on calcium carbonate single crystal and particle surfaces at the adsorbed water carbonate interface, Physical Chemistry Chemical Physics 9 (2007) 3011–3024.
[39] N. Fairley, CasaXPS Version 2.3.17dev4-8, 1999–2013.
[40] B. Ranby, J.F. Rabek, Photodegradation, Photo-oxidation and Photostabilization of Polymers: Principles and Applications, Wiley-Interscience, New York, NY, 1975.
[41] E. Pretsch, P. Buehlmann, M. Badertscher, Structure Determination of Organic Compounds: Tables of Spectral Data, Springer, Berlin, Germany, 2009.
[42] B.H. Stuart, Infrared Spectroscopy—Fundamentals and Applications. (Analytical Techniques in the Sciences (AnTs)), John Wiley & Sons, Chichester, UK, 2004.
[43] L.V. Azaroff, Elements of X-Ray Crystallography, McGraw-Hill, New York, 1968.
[44] S. Shukla, S. Seal, S.R. Mishra, Synthesis and characterization of silver sulfide nanoparticles containing sol–gel derived HPC-silica film for ion-selective electrode application, Journal of Sol-Gel Science and Technology 23 (2002) 151–164.
[45] G. Hota, S.B. Idage, K.C. Khilar, Characterization of nano-sized CdS–$Ag_2S$ core–shell nanoparticles using XPS technique, Colloids and Surfaces A: Physicochemical and Engineering Aspects 293 (2007) 5–12.
[46] A.S. Manocha, R.L. Park, Flotation related ESCA studies on lead(II) sulfide surfaces, Applied Surface Science 1 (1977) 129–141.
[47] K.M. Abraham, S.M. Chaudhri, The lithium surface film in the lithium/sulfur dioxide cell, Journal of the Electrochemical Society 133 (1986) 1307–1311.
[48] D. Gonbeau, C. Guimon, G. Pfister-Guillouzo, A. Levasseur, G. Meunier, R. Dormoy, XPS study of thin films of titanium oxysulfides, Surface Science 254 (1991) 81–89.
[49] J. Baltrusaitis, D.M. Cwiertny, V.H. Grassian, Adsorption of sulfur dioxide on hematite and goethite particle surfaces, Physical Chemistry Chemical Physics 9 (2007) 5542–5554.
[50] R. Ivanauskas, J. Baltrusaitis, Synthesis and surface properties of polyamide–$Cu_xSe$ composite thin films, Applied Surface Science 283 (2013) 360–366.
[51] A.J. Frueh Jr., The crystallography of silver sulfide, $Ag_2S$, Zeitschrift für Kristallographie, Kristallgeometrie, Kristallphysik, Kristallchemie 110 (1958)136–144.
[52] I. Martínez-Ruvalcaba, J.F. Hernández-Paz, J.R. Farías Mancilla, P. Piza Ruiz, C.A. Martínez Pérez, P.E. García-Casillas, C.A. Rodríguez-González, Optical properties of bio-inspired silver sulfide structures, Journal of Alloys and Compounds 586 (2014) S526–S530.
[53] S. Dowland, T. Lutz, A. Ward, S.P. King, A. Sudlow, M.S. Hill, K.C. Molloy, S.A. Haque, Direct growth of metal sulfide nanoparticle networks in solid-state polymer films for hybrid inorganic–organic solar cells, Advanced Materials 23 (2011) 2739–2744.
[54] N. Mukherjee, S. Jana, G.G. Khan, A. Mondal, Photo-induced exciton generation in polyvinylpyrrolidone encapsulated $Ag_2S$ core–shells: electrochemical deposition, regular shape and high order of particle size distribution, Journal of Applied Physics 112 (2012) 124324–124326.
[55] E.S. Smotkin, C. Lee, A.J. Bard, A. Campion, M.A. Fox, T.E. Mallouk, S.E. Webber, J.M. White, Size quantization effects in cadmium sulfide layers formed by a Langmuir–Blodgett technique, Chemical Physics Letters 152 (1988) 265–268.
[56] H. Schönherr, D. Snétivy, G.J. Vansco, A nanoscopic view at the spherulitic morphology of isotactic polypropylene by atomic force microscopy, Polymer Bulletin 30 (1993) 567–574.